

Possible molecular bottom-up approach to optical metamaterials

X. W. Sha,¹ E. N. Economou,^{1,3} D. A. Papaconstantopoulos,¹ M. R. Pederson,² M. J. Mehl,² and M. Kafesaki³

¹*School of Physics, Astronomy, and Computational Sciences, George Mason University, Fairfax, Virginia 22030, USA*

²*Center for Computational Materials Science, Naval Research Laboratory, Washington, District of Columbia 20375, USA*

³*Foundation for Research and Technology Hellas, P.O. Box 1385, 71110 Heraklion, Crete, and University of Crete, Greece*

(Received 9 February 2012; published 4 September 2012)

We investigate the possibility of a molecular bottom-up approach to the construction of the basic element for optical negative index metamaterials. Undoped and doped graphene-based molecules, including nanotubes, are considered. We employ first-principles and tight-binding electronic structure methods to determine the energy levels and the stability of the molecules. Under certain assumptions, we simulate the electromagnetic response of the molecules by a corresponding network of perfect wires. The nanotubes exhibit a resonant response at the soft x-ray range.

DOI: 10.1103/PhysRevB.86.115404

PACS number(s): 78.67.Wj, 73.22.Pr, 42.25.Bs, 71.15.Nc

I. INTRODUCTION

One of the most exciting and promising developments in basic physics, applied physics, and engineering is the endowment of photons with revolutionary propagation and spectral properties through their interaction with novel artificial materials (LHMs) or, more generally, **negative** index metamaterials (NIMs).¹⁻⁴ LHMs are tailored man-made structures composed of subwavelength building blocks (“photonic atoms”); the latter exhibit a resonant magnetic response leading to the full exploitation of the magnetic component of the electromagnetic (EM) field and, as a result, to the possibility of a negative effective permeability.⁵ This negative permeability is combined with a negative permittivity response, quite common in metallic structures, thus producing negative index of refraction behavior¹ in those materials over a frequency range that can reach near or at the visible spectrum.⁶⁻⁸ The negative permeability is achieved by a resonance strong enough to overcompensate for the v/c factor inherent in the magnetic response of the “photonic atoms.” As a result of negative permeability and permittivity, properties that were unthinkable before are exhibited or predicted:¹⁻³ opposite phase and energy velocities; negative index of refraction (NIMs can act as optical antimatter); inverse Doppler shift; reverse Cerenkov radiation; negative radiation pressure; flat lenses; and almost perfect lenses,⁹ where the diffraction limit is no obstacle to an almost perfect focusing, at least in principle.

Several designs toward the goal of negative index have been developed over the past ten years.⁷⁻¹⁵ Their unit cell combines metallic elements placed on dielectric substrates. A particularly important example of a component of such a photonic “atom” is the so-called split-ring resonator (SRR) (see Fig. 1).⁵ SRR is essentially a tiny electromagnet consisting of a metallic wire of split-ring or U shape, possessing both self-inductance L and capacitance C and, therefore, a natural frequency $\omega_o = 1/\sqrt{LC}$. Since both L and C are proportional to the size ℓ of the SRR, the resonance frequency ω_o is expected to be inversely proportional to ℓ or, equivalently, to the size of the unit cell. For sizes less than 100 nm, ω_o enters the visible spectrum. However, as the size of the SRR enters the nanoregime, i.e., as it becomes smaller than or about equal to 100 nm in order to approach the visible part of the spectrum, several difficulties appear:¹⁶

(1) To the usual current I related magnetic energy, $L_m I^2/2$, another term proportional to I^2 is added. This term, which is usually negligible at microwaves, is due to the kinetic energy of the current-carrying electrons,¹⁶⁻¹⁹

$$\frac{1}{2} N_e m_e v_s^2 \equiv \frac{1}{2} L_e I^2, \quad (1.1)$$

where Eq. (1.1) is the definition of the kinetic (electron) self-inductance L_e ,¹⁶⁻¹⁹ and v_s is the average systematic velocity of the electrons, which is proportional to the current I . Taking into account that $N_e = n_e \ell S$ and $I = S n_e e v_s$, where n_e is the concentration of the free electrons, $S = wt$ is the cross section of the metallic wire, and ℓ ($=4d-g$) is its length (see Fig. 1), we find that $L_e = m_e \ell / n_e e^2 S$ is inversely proportional to the size of the unit cell (assuming that all lengths scale proportional to the lattice constant a). The ratio $n_e e^2 / m_e$ can be expressed in terms of the plasma frequency ω_p (at which the metallic dielectric function vanishes): $n_e e^2 / m_e = \epsilon_b \omega_p^2 \epsilon_o$, where ϵ_b is due to the bound electrons, and it is approximately a constant larger than 1 (for silver $\epsilon_b = 6.8$); and ϵ_o is the permittivity of the vacuum. To compare the kinetic self-inductance L_e to the magnetic one, L_m , we need the textbook expression for $L_m = (\mu_o \ell / 2\pi) [\ln(4\ell/\pi b) - 1.5]$,²⁰ where μ_o is the permeability of the vacuum, and the cross-section S , which is usually rectangular (wt), is written here as $S \equiv \pi b^2$. Taking into account the above expression for L_m , we find

$$L_e/L_m = (\lambda_p^2/S) \{2\pi \epsilon_b [\ln(4\ell/\pi b) - 1.5]\}^{-1}, \quad (1.2)$$

where $\lambda_p \equiv 2\pi c/\omega_p$. Writing the volume of the unit cell as $a \times a \times a_z$ (a_z is the unit cell size in the direction perpendicular to the SRR plane) and taking the following typical values for an SRR, $\ell = 2.8 a$, $t = 0.05 a$, $b = 0.04 a$, $w = 0.1 a$, $a_z = 0.2 a$, $S = 0.005 a^2$, we obtain $L_e/L_m \approx \lambda_p^2/128S \approx 1.56 \lambda_p^2/a^2$. For silver, for which $\lambda_p = 326$ nm, $L_e = L_m$ when $a \approx 400$ nm. Taking into account that a typical value of SRR capacitance is $C = 0.3 \epsilon_o a$,²⁰ we find that the resonance frequency is

$$\begin{aligned} \omega_o &= \frac{1}{\sqrt{C(L_m + L_e)}} = \frac{1}{\sqrt{C L_m [1 + (L_e/L_m)]}} \\ &\approx \frac{1.57c}{\sqrt{a^2 + 1.56 \lambda_p^2}}, \end{aligned} \quad (1.3)$$

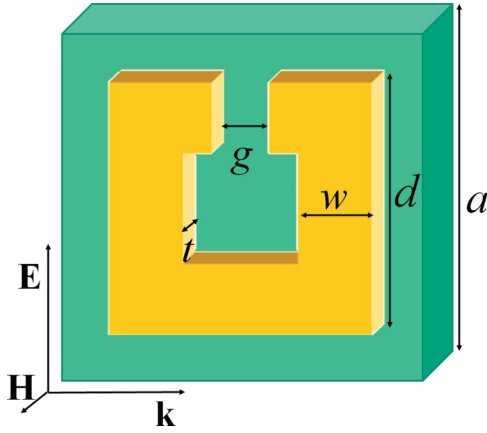


FIG. 1. (Color online) A typical single-ring SRR with a single gap. The substrate (green/medium gray) is a dielectric, and the ring (yellow/light gray) is metallic.

which shows that the relation $\omega_o \propto a^{-1}$ breaks down if a becomes comparable to λ_p , and eventually ω_o saturates to about $0.2\omega_p$, which usually is in the near infrared. To face this limitation, we can decrease the value of the capacitance by making the split larger or by including more splits.¹⁶ For example, if we include four splits instead of one (all of equal size g), the saturation value will be increased by a factor of 2, enough for entering the red part of the visible spectrum, if the silver value for ω_p is used.

(2) The second difficulty appearing in the regime $a \approx 100$ nm is related to the strength of the resonance. The latter needs to be strong enough to produce negative values of the permeability or, equivalently, values of the susceptibility χ_m smaller than -1 . The susceptibility is given by the following expression:²⁰

$$\chi_m(\omega) = -\frac{F\omega^2}{\omega^2 - \omega_o^2 + i\omega R/L}. \quad (1.4)$$

In this formula, $R = \ell/(S\epsilon_b\epsilon_o\omega_p^2\tau)$ is the resistance of the metallic wire, τ is the relaxation time (for silver, $\hbar/\tau \approx 0.04$ eV), $R/L \approx R/L_e = 1/\tau$, and F is a measure of the strength of the resonance. F is given by¹⁷

$$F = \frac{(\ell/4)^4 \mu_o}{a^2 a_z L} \approx \frac{(\ell/4)^4 \mu_o}{a^2 a_z L_e} \approx \frac{\pi^2 \ell^3 \epsilon_b S}{64 a^2 a_z \lambda_p^2}. \quad (1.5)$$

It is easy to show that the minimum of the real part of $\chi_m(\omega)$ appears at $\omega - \omega_o \approx 1/2\tau$, and its value at the minimum is approximately $-F\omega_o\tau/2$. Substituting in the latter result the explicit values we have used before and taking $a = 100$ nm and the silver values for ω_p and τ , we find $-F\omega_o\tau/2 \approx -2.57$. Taking into account Eq. (1.5), which implies that F is proportional to $S \propto a^2$, we conclude, following the same reasoning, that $-F\omega_o\tau/2$ will become larger than -1 for a smaller than 63 nm. Hence, the unit cell size must be larger than 63 nm in order to produce negative values of the permeability. Actually, the situation is worse than that: The ratio r of the real part to the imaginary part of the susceptibility is approximately equal to $2(\omega - \omega_o)\tau$, which for the value of $\omega - \omega_o$ corresponding to the minimum of $\text{Re}\chi_m(\omega)$ gives $\text{Re}\chi_m(\omega)/\text{Im}\chi_m(\omega) \approx -1$. It is obvious that such a level of

ohmic losses is unacceptable for any application. The latter requires that the above ratio $|r|$ must be of the order of ten or so. Thus, the operational frequency ω_1 must satisfy the relation $\omega_1 - \omega_o = |r|/2\tau \ll \omega_o$, and then the requirement $\text{Re}\chi_m(\omega_1) < -1$ leads to the relation $F\omega_o\tau > |r| \approx 10$.

There are two ways to satisfy this last relation. The first one is to increase F by increasing the size of the unit cell to about $a \approx 140$ nm. However, in this case, the frequency ω_o will be no higher than the near infrared; the corresponding wavelength $\lambda_o = 2\pi c/\omega_o$ would be no lower than 1000 nm. The other possibility is to increase τ beyond its value for silver. However, silver is the best conductor among all elemental metals or compounds.

(3) The third difficulty, namely, that of the ohmic losses in the metallic parts, presents the most serious obstacle in achieving operational LHM in the visible part of the spectrum. Several approaches have been followed in dealing with this problem, from the obvious one of optimizing the geometrical structure parameters, to coming up with improved designs,^{21,22} to more elaborate ones such as exploiting the interaction of different resonances to minimize losses, as in the electromagnetically induced transparency approach.²³ Although some progress has been achieved, the basic problem remains. Recently, the idea of incorporating active elements in the building blocks of LHM has been pursued.^{24–28} The aim is to compensate to some extent for the ohmic losses by supplying external energy. This promising approach is not without some difficulties.

In this paper, we explore a radically different approach from the traditional top-down path to achieve high-frequency (e.g., optical) magnetism and thus high-frequency LHMs. Our approach is in the direction of bottom-up, i.e., of employing molecular structures of increasing size as the building blocks of LHM.

II. OUTLINE OF OUR APPROACH

Molecular structures, as opposed to the metallic ones, have two advantages, at least in principle. The electronic transport can be ballistic and not diffusive as in metals. This is expected to avoid the problem of ohmic losses altogether. Furthermore, the molecules can be close-packed so as to decrease drastically the size of the unit cell in the perpendicular direction a_z relative to all other geometrical lengths and, therefore, increase the value of F [see Eq. (1.5)].

However, the molecular approach is not without serious challenges. First, as the molecule becomes larger, i.e., linear size of about 10 nm or more, the question of stability of the desired shape arises. Second, if the analogue of the metallic SRR is pursued, there is a need to implement the interruption of free electronic flow at some point, i.e., to create the analogue of the split in SRR. Third, this implemented interruption must be immune to quantum tunneling so as to avoid leakage. Fourth, the role of the substrate may not be negligible. Fifth, the feasibility of synthesizing the proposed molecules has to be examined. Finally, the crucial assumption of ballistic electronic transport has to be checked under realistic conditions.

To face the problem of stability, we limited ourselves to graphene-based molecules including nanotubes, with hydrogen atoms to passivate the dangling bonds at the edges.

Graphene sheets of relatively large size are known to be stable in their almost planar configurations. Moreover, in the next section (Sec. III), we examined the stability for several molecules starting from the simple benzene (C_6H_6) and proceeding to much larger quasicircular pieces of graphene-based molecules containing up to 7000 C atoms, by combining various arrangements of the basic hexagonal benzene ring. For molecules up to 100 atoms, we employed the Naval Research Laboratory Molecular Orbital Library (NRLMOL), a sophisticated all-electron first-principles density functional theory (DFT) approach mainly developed by one of us (M. R. P.), where a variational ansatz is made and the wave functions are expanded in terms of Gaussian-type orbitals.²⁹ This approach allows, besides the determination of energy levels and the corresponding eigenfunctions, relaxation of the initial structure using the conjugate-gradient method, and hence, it is capable of checking the stability of the structure. To implement the analogue of the split in the SRR, we replaced one or more of the carbon atoms by various foreign atoms. The latter must be as effective as possible in interrupting the electronic flow and at the same time must produce a minor perturbation in the planar structure of the initial molecule. Among the various substitutional atoms we tried, nitrogen seems to be the one to satisfy the second requirement and perhaps the first one as well. As we shall show later herein, trivalent atoms, such as boron, seriously affect the in-plane bonding, but they produce negligible out-of-plane distortions.

For molecules larger than 100 atoms, we used the Naval Research Laboratory tight-binding (NRLTB) method.^{30–32} The TB parameters for the C-H system that we used are those reported in our previous publications,^{33,34} where the C-C interactions are fit to linearized augmented plane-wave results for diamond, graphite, simple cubic structures, and to the NRLMOL results of C_2 dimer; the H-H interactions are fit to molecular energy levels of H_2 and an H_6 ring; and the C-H interactions are obtained by fitting to the NRLMOL energy levels and total energies of methane, ethane, and benzene molecules while freezing the C-C and H-H parameters. These parameters are used in TB calculations of larger systems, including relaxation, and show excellent transferability, as discussed in the next section.

The big advantage of the NRLMOL method is its first-principles reliable results, including not only energy levels but eigenfunctions as well, and hence absorption coefficients. It is generally accepted that methods based on the DFT are by far the most accurate within the independent effective particle scheme. The price one pays for such reliability is limitations in the size of the systems that can be studied. Roughly speaking nonsymmetric molecules or unit cells in solids consisting of more than 100 atoms cannot be treated with DFT-based methods. On the other hand, the TB or linear combination of atomic orbitals (LCAO) method allows us to treat systems consisting of the order of 10,000 atoms and at the same time permits a relatively simple physical interpretation of the results obtained. The disadvantage of the various TB methods is that the required matrix elements have to be fitted to the results of some other reliable method such as the NRLMOL. Thus, to reach the large molecules needed in our case, we have to combine both methods in our calculations, namely, the NRLMOL and the NRLTB.

Also in Sec. III, we simulate the performance of the most promising molecules under the action of an incoming plane electromagnetic wave by an equivalent network where each bond between two nearest neighbor carbon atoms has been replaced by a perfect metallic wire, and each foreign atom together with its bonds has been removed from the network. The geometrical parameters of the simulation network are kept the same as in the actual molecule. This drastic approximation became almost obligatory, because of the great difficulty of doing a quantum mechanical calculation in a system containing at least several tens of atoms and in the presence of a time-dependent electromagnetic field. In Sec. IV, we discuss the consequences of this approximation. The network allows us to determine, by solving numerically Maxwell's equations through the finite integration technique (employed through CST Microwave Studio software), its transmission and reflection amplitudes, the distribution of the currents, and the distribution of the electric and magnetic fields. These numerical data are expected to be in gross agreement with the actual experimental data from the real molecule, if the assumptions of no tunneling through the foreign atoms and the ballistic transport are valid. To justify at least partially this last statement, we perform several quantum mechanical calculations, which, in the absence of electron-phonon interactions, confirm the ballistic character of the transport and hence lead to an almost zero resistance flow up to very high frequencies associated with substantial interband transitions (see Sec. IV).

In Sec. V, we discuss and check some of the other assumptions made in this work.

III. RESULTS FOR GRAPHENE-BASED MOLECULES

In Fig. 2, we show the calculated energy levels of benzene using the first-principles methods NRLMOL and NRLTB. Since the first-principles benzene energy levels have been included in the fitting of the TB Hamiltonian, it is not surprising to see a nearly perfect agreement between NRLMOL and NRLTB energy levels. Both NRLMOL and NRLTB predict a large highest occupied molecular orbital–lowest unoccupied molecular orbital (HOMO–LUMO) energy gap of 5.09 eV, which is in rather good agreement with the experimental value of 4.90 eV.

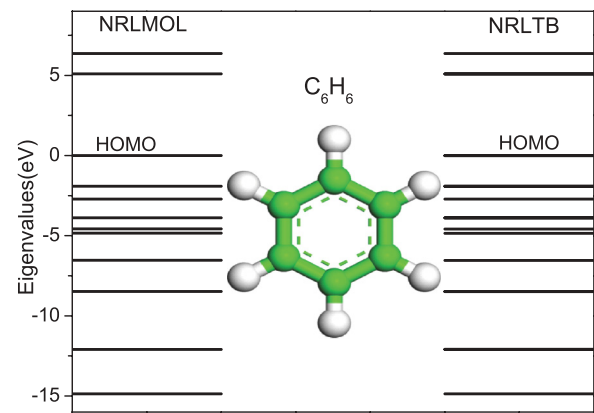


FIG. 2. (Color online) Excellent agreement in the energy levels of benzene is achieved between the first-principles NRLMOL method and the NRLTB approach.

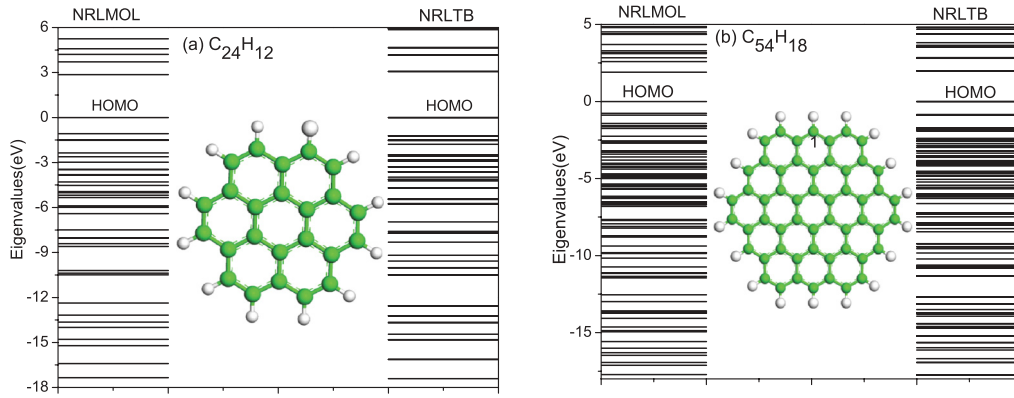


FIG. 3. (Color online) Two hexagonal pieces of graphene terminated with hydrogen “decoration” to eliminate dangling bonds at the edges. In the presence of an ac magnetic field perpendicular to the plane of the molecules, an ac is expected to circulate along the edge carbon atoms.

In Fig. 3, we compare the NRLMOL and NRLTB energy levels for two larger hexagonal pieces of graphene with the edge carbon bonds passivated by hydrogen atoms. We gradually increase the number of benzene rings of the structure: $C_{24}H_{12}$ has six peripheral benzene rings, and $C_{54}H_{18}$ has twelve peripheral rings. Both molecules are stable and remain planar structures after optimization. The energy levels predicted by NRLTB for both molecules agree reasonably well with NRLMOL results. In particular, the NRLTB HOMO-LUMO gaps, 3.06 eV for $C_{24}H_{12}$ and 1.99 eV for $C_{54}H_{18}$, are in rather good agreement with the corresponding NRLMOL gaps, 2.86 eV and 1.90 eV, respectively. This agreement of the energy levels, including the size of the gap, calculated by the NRLTB and NRLMOL methods indicates the good transferability of our TB Hamiltonian. Notice that the electronic structure of these graphenelike molecules, such as the HOMO-LUMO energy gap, strongly depends on system size. Benzene, $C_{24}H_{12}$, and $C_{54}H_{18}$ all have large HOMO-LUMO gaps, significantly different from the gapless feature of bulk graphene. The HOMO-LUMO gap significantly decreases with an increase in molecular size, from 1.99 eV in $C_{54}H_{18}$ to 0.11 eV in $C_{726}H_{66}$, as shown in Fig. 4. With further increase in the system size, containing over 800 C atoms, the molecule essentially becomes gapless, as in bulk graphene. The largest systems we examined, $C_{5046}H_{174}$ and $C_{6936}H_{204}$, are both stable and have essentially zero HOMO-LUMO gap. Being able to run these calculations for systems with over 7000 atoms is a unique capability of our NRLTB method.

As discussed in the Introduction, the stability of the molecule, as its size gets bigger, is crucial in designing the LHMs. We use the NRLTB approach and the conjugate gradient method to optimize 16 graphenelike molecules, with the number of the peripheral benzene rings along each hexagon side varying from 12 to 198. After the optimization (i.e., the rearrangements of the coordinates of the atoms as to minimize the total energy), all the molecules remain stable in graphenelike structures.

To further check the stability of the graphenelike molecules at finite temperature, we perform a TB molecular dynamics simulation on a $C_{864}H_{72}$ molecule at 300 K for 8000 time steps, with each time step corresponding to 0.5 femtosecond. The average radial distribution function,³³ as shown in Fig. 5, does not show any substantial changes with the increase in

simulation time, indicating the stability of the molecule at room temperature.

If there are 600 peripheral benzene rings in graphenelike structures, then the diagonal length of the molecule would be about 24 nm. The interesting feature of this structure is its expected response to the presence of an alternating current (ac) magnetic field perpendicular to the plane of the molecule. Such a field will induce a circulating current in each benzene ring. The currents at each bond shared by two neighboring rings are equal in magnitude and of opposite direction. Thus, they are expected to cancel each other. The only current that will survive is the one along the edge carbon-carbon bonds, which belong to the peripheral benzene rings. Thus, an ac edge current will circulate. This picture is confirmed by the explicit numerical calculation in the simulating network. As shown in Fig. 6(a), the current is running across the edge of the network, although the cancelation in the internal bonds is not quite perfect.

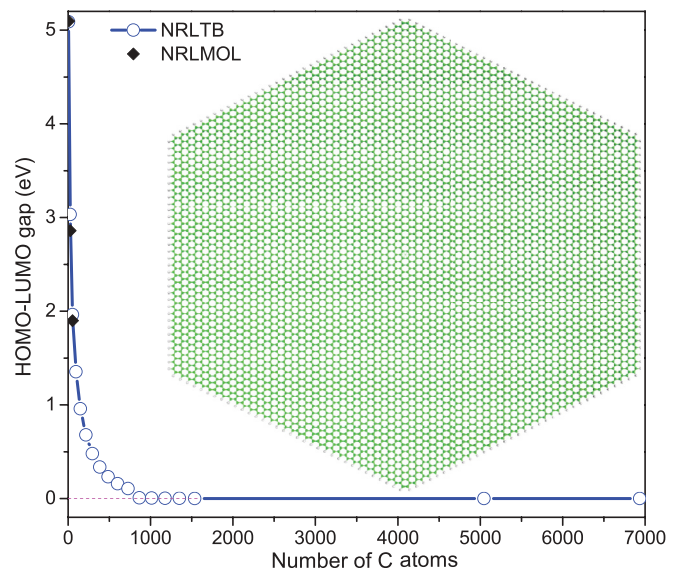


FIG. 4. (Color online) The HOMO-LUMO energy gap decreases gradually with the increase in the size of the graphene-based molecule, until the gap vanishes for molecules containing more than 800 C atoms. This result is consistent with the zero gap of graphene.

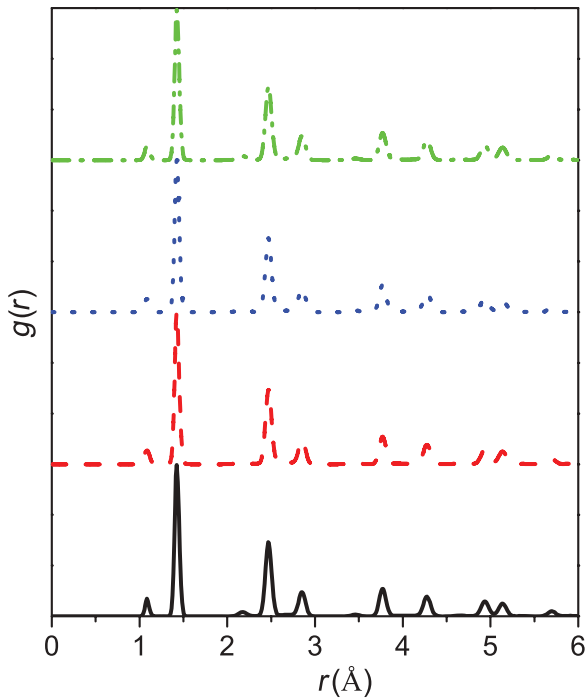
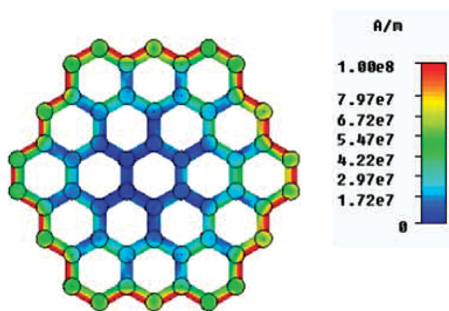


FIG. 5. (Color online) The evolution of the radial distribution function $g(r)$ of a $C_{864}H_{72}$ molecule in a TB molecular dynamics simulation. The solid, dashed, dotted, and dashed-dotted lines represent the average values during the 0–0.5, 0.5–1.0, 1.0–1.5, and 1.5–2.0 picosecond simulation times, respectively.

If we examine the permeability of a dense square lattice of such rings as the ones in Fig. 6(a) (of nearest neighbor distance two times the bond length) under the influence of an ac magnetic field perpendicular to the plane of the structure, we find that at low frequencies μ is ~ 0.6 , due to the partial cancellation of the external field by the field induced by the circular current. This permeability can become much smaller, if we place the rings in a hexagonal-close-packed (hcp) lattice



(a)

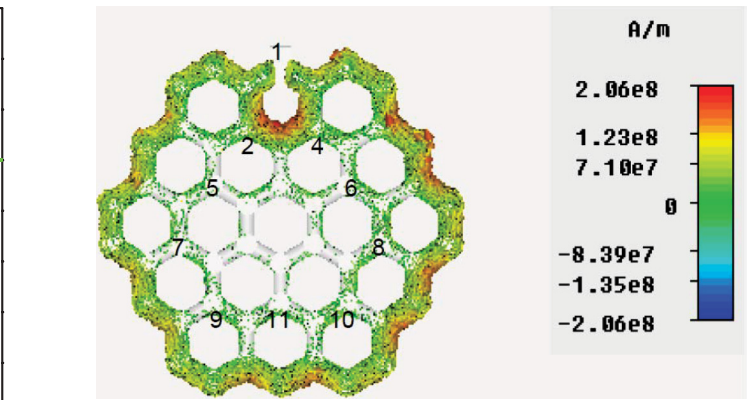
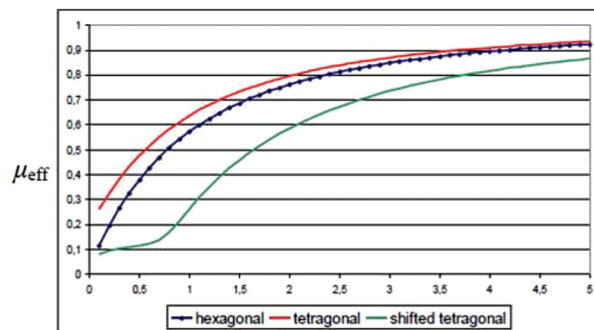


FIG. 7. (Color online) If site 1 in the structure of Fig. 3(b) is blocked, the edge current induced by an ac magnetic field will not be interrupted, since it will follow the alternative path involving sites 2 and 4 instead of site 1.

or in a shifted-tetragonal lattice, reaching values as low as 0.2. The possibility of achieving low effective permeability values using closed-current loops is illustrated in Fig. 6(b), where we have approximated the molecules of Fig. 6(a) by perfect metallic circular rings, and we show the magnetic permeability of a system of such rings in various lattice arrangements and distances.

If we could interrupt the edge current of the network shown in Fig. 6(a) at one site, without diverging it to other directions, we could have an excellent molecular SRR. Unfortunately, if we replace the carbon atom labeled 1 in $C_{54}H_{18}$ shown in Fig. 3(b) by a nitrogen atom, and even if we assume that the nitrogen atom would fully block the flow through site 1, still the flow will not be interrupted, since it can follow an alternative path that bypasses site 1 as shown in Fig. 7. Figure 7, which shows how the current is flowing (according to the numerical solution of Maxwell’s equations) in the simulated network with site 1 removed, indicates that to create a SRR-like response, all the internal continuous current paths of the molecule should be eliminated. A possibility of



(b)

FIG. 6. (Color online) (a) Current flow at the network simulating the molecule shown in Fig. 3(b), according to the numerical solution of Maxwell’s equations. The red (dark gray) color indicates the regions of larger current, showing a circular current flow mainly along the edge of the network. (b) Effective permeability for a periodic system of perfectly conducting circular rings of radius r_0 , placed in a hexagonal (middle curve, blue online), tetragonal (upper curve, red online), and shifted-tetragonal (lower curve, green online) lattice (the shift consists of a scenario where every second layer in the direction perpendicular to the rings-plane [i.e., the z direction] is displaced by half the lattice constant along the x and y directions). da is the in-plane distance between the rings (distance of closer points of two neighboring rings along the x and y directions). The distance along the z direction is equal to $0.1r_0$.

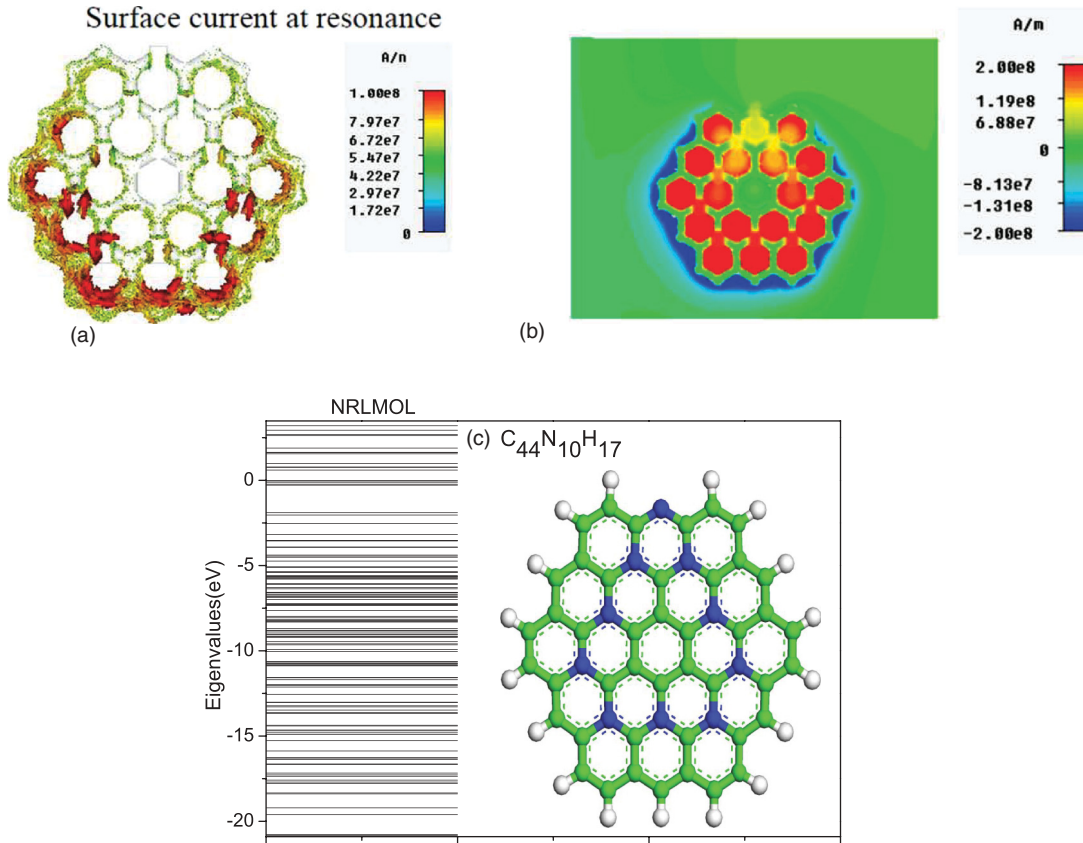


FIG. 8. (Color online) (a) The surface current, at the magnetic resonance frequency, flowing in a network as in Fig. 7 but with the sites 1, 2, and 4–11 removed so that no closed benzene loop has been left. (b) Magnetic field (perpendicular to the plane of the network) created by the current flow of panel (a); this field is of opposite direction inside and outside the molecule. (c) The optimized structure and electronic structure of such a network calculated from NRLMOL.

eliminating all alternative continuous current paths arises if all the labeled sites in Fig. 7 are blocked or removed, as shown in Fig. 8. The molecular structure remains stable with the substitution of all these carbon atoms by nitrogens, as shown by the first-principles NRLMOL optimization [see Fig. 8(c)]. In this case, a resonance in the permeability (followed by

negative permeability values) in a square periodic system of molecules appears at wavelength $\sim 7.5a$ (a is the linear size of the molecule), coming from a resonant looplike current, as shown in Fig. 8(a).

Another molecule that can act as a molecular SRR is the hollow graphene-based one, shown in Fig. 9(a), with

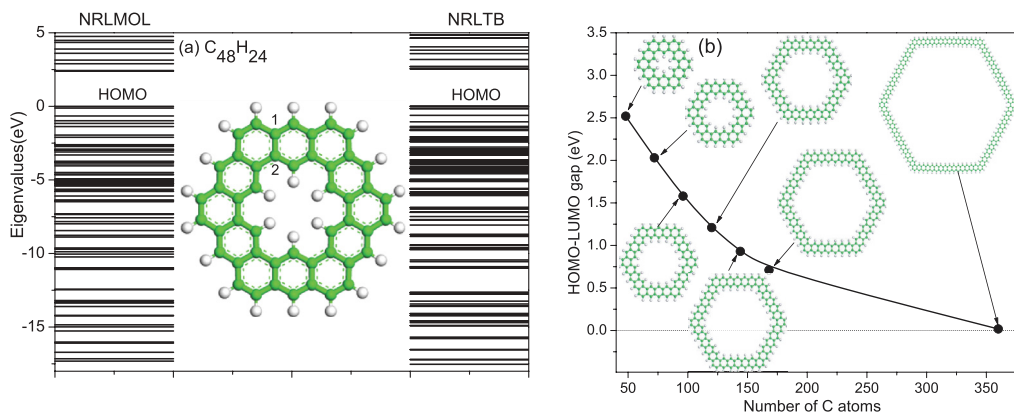


FIG. 9. (Color online) (a) A hollow nitrogen-doped graphene molecule, which is a credible candidate for a molecular SRR, if a split could be introduced that would block the flow at sites 1 and 2. This blocking can possibly be achieved by replacing carbon atoms labeled 1 and 2 (and neighboring carbon atoms, if necessary) by nitrogen atoms. (b) The ring structure remains stable as the molecular size increases, as shown by the TB conjugate-gradient optimizations. Such hollow graphene molecules are stable for systems containing hundreds of atoms, as shown by our TB optimization calculations.

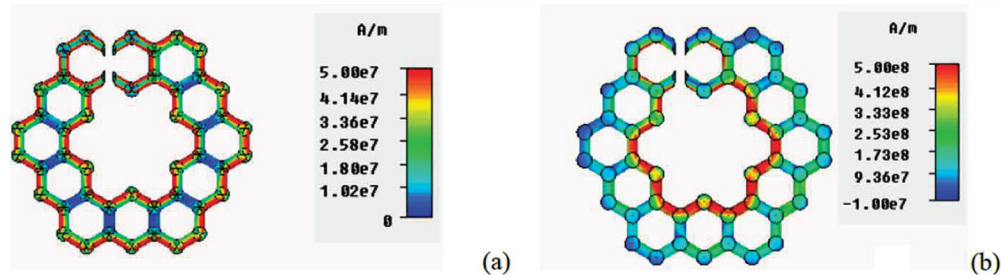


FIG. 10. (Color online) Surface current density for the hollow graphene structure of Fig. 9(a), with sites 1 and 2 blocked, at frequencies well below the magnetic resonance frequency. (a) The current is flowing both at the inner and the outer edges. (b) At the magnetic resonance frequency, the current is flowing almost exclusively at the inner edge.

the carbon dangling bonds, inner and outer, passivated by hydrogens, and atoms 1 and 2 replaced by nitrogen. If a single pair of dopants is not capable of breaking the flow, two or three such pairs next to each other will suffice. In Fig. 9(b), stable hollow molecules similar to the one shown in Fig. 9(a), but of larger size, are shown together with their LUMO-HOMO gap. An ac magnetic field normal to the plane of the molecule shown in Fig. 9(a) is expected to induce a resonant looplike current showing two distinct behaviors: For frequencies well below the resonance, the current flow goes around the external edge, continues through the break, and enters the internal edge, goes around it in the opposite direction and joins continuously the external edge through the break [see Fig. 10(a)]. However, as shown in Fig. 10(b), the situation is different at the resonance frequency, where the current is essentially running back and forth along the internal edge of the structure.

A very interesting molecular case is the nanotube (Fig. 11) with the incoming linearly polarized electromagnetic wave propagating along the axis of the tube. Because this molecule is three dimensional (3D), both the electric and the magnetic field components may influence the current flow, in contrast to the planar molecules considered before, where only the ac magnetic field will determine the current. At first sight and on the basis of the magnetic field only, it is expected to have

benzene loop currents mainly in the loops perpendicular to the magnetic component of the incoming radiation and no current in the benzene rings parallel to the magnetic field. Thus, two symmetric splits are expected at the front and the back ends of the nanotube. The current at the front and the back end of the tube will flow in opposite directions, if the phase difference of the incoming EM fields at the two ends is negligible. However, if the length ℓ of the tube were equal to $\lambda/2$ (λ is the wavelength of the EM field within the tube), the two end currents would be expected to run in the same direction. The actual behavior is more complicated, if the cancellations and the noncancellations of the current flows in each benzene loop are examined more carefully by taking into account the role of the electric field as well. Indeed, the numerical calculation in the network simulating the nanotube (where the C-C bonds are considered as perfect metallic wires) shows a pattern as seen in Fig. 12: In column (a) of Fig. 12, the j_y and j_z components of the current are shown for the case of the wavelength being much larger than the length a of the tube (for a detailed description, see the caption of Fig. 12). The case of $\lambda/2 \approx a$ is shown in column (b) of Fig. 12 and is described in its caption.

In Fig. 13, we plot the electromagnetic response (transmission and reflection amplitudes) of the nanotube shown in

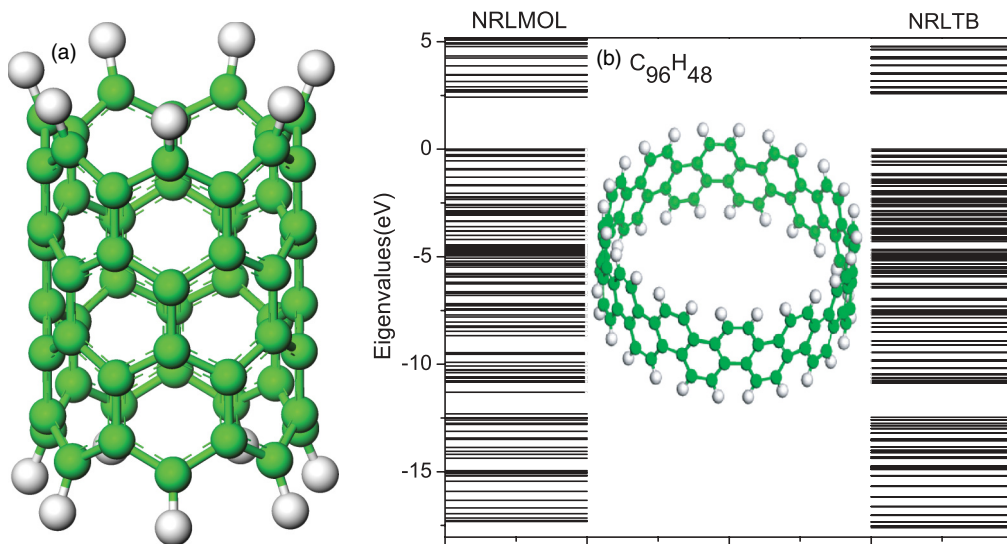


FIG. 11. (Color online) (a) The nanotube, the EM response of which is studied, under a linearly polarized EM field propagating along its axis. (b) The optimized configuration and energy levels of a small nanotubelike structure. NRLTB reproduced well the electronic structures predicted by NRLMOL.

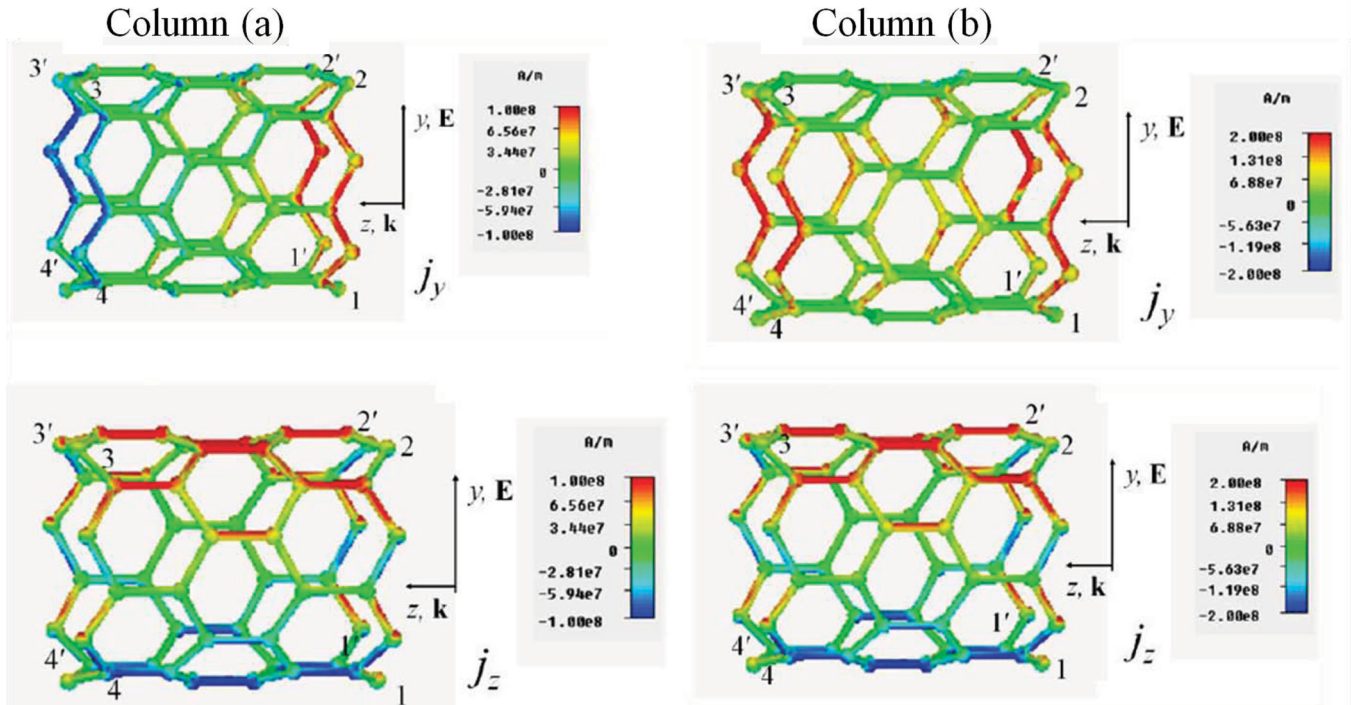


FIG. 12. (Color online) Column (a) The j_y (top panel) and j_z (bottom panel) components of the current for an EM wave propagating along the axis of the nanotube of Fig. 11(a), for the case where the wavelength is much longer than the length, a , of the tube. In this case, the current flows from 1 to 2 and from 1' to 2' in phase mostly along the y direction. It continues from 2 to 3 and from 2' to 3' mostly in the z direction, and then from 3 to 4 and from 3' to 4', in the opposite y direction; finally, from 4 it returns to 1 and from 4' it returns to 1'. In the case of $\lambda/2 \approx a$, column (b), all currents from 1 to 2, from 1' to 2', from 4 to 3 and from 4' to 3' run almost in phase along the y direction; the currents from 2 to 3 and from 2' to 3' run in the opposite direction to the ones from 1 to 4 and from 1' to 4'.

Figs. 11(a) and 12. Notice the strong resonance response at $a/\lambda_0 \approx 0.6$ (λ_0 is the free-space wavelength), which for the length $a \approx 7 \text{ \AA}$ of the system in Fig. 12 is at the soft x-ray

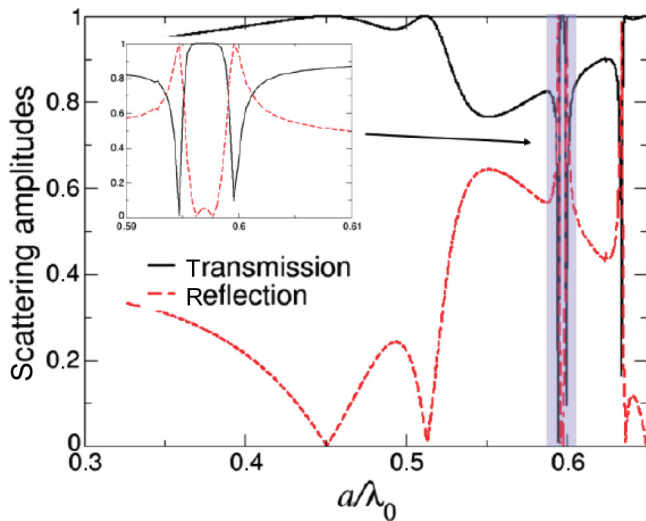


FIG. 13. (Color online) The transmission (black solid line) and reflection (red dashed line) amplitudes for a linear EM wave propagation along the axis of the nanotube shown in Figs. 11(a) and 12, consisting of perfect metallic wires. The length of the nanotube is a , and λ_0 is the free-space wavelength. The resonance response at $a/\lambda_0 \approx 0.6$ (shadowed region) is magnified in the inset.

regime, $\hbar\omega \approx 1060 \text{ eV}$. This strong response is unexpected and important because matter is usually responding very weakly to x rays. Thus, we predict that single-wall carbon nanotubes may respond resonantly to soft x rays. This prediction is based upon the assumed stability of the nanotube and the expected ballistic propagation of its free electrons. The first of these aspects is confirmed by our calculations, which show that, in addition to the good transferability of our TB Hamiltonian in predicting the structural and electronic structure properties of the planar graphenelike structure, our NRLTB reproduces well the NRLMOL optimized structural and energy level characters of $C_{96}H_{48}$, a small molecule of nanotubelike structure, as shown in Fig. 11(b). The HOMO-LUMO gap of 2.58 eV predicted by NRLTB is in reasonable agreement with the value of 2.43 eV calculated from NRLMOL. The good transferability enables us to study large nanotubelike molecules containing thousands of carbon atoms. Such a study is a must given the unexpected strong response shown in Fig. 13.

Among the various molecular structures considered in this paper, the most promising is the ring type shown in Fig. 9 and the nanotube type shown in Fig. 11. Single-wall nanotubes can be synthesized almost routinely, and they do not involve uncertainties regarding possible adverse effects associated with the presence of an unavoidable substrate. Their almost ballistic transport has been accepted.

The ring molecules of Fig. 9 do not seem to present major difficulties in their synthesis, since each linear segment can be obtained by straight polymerization of benzene rings. The six

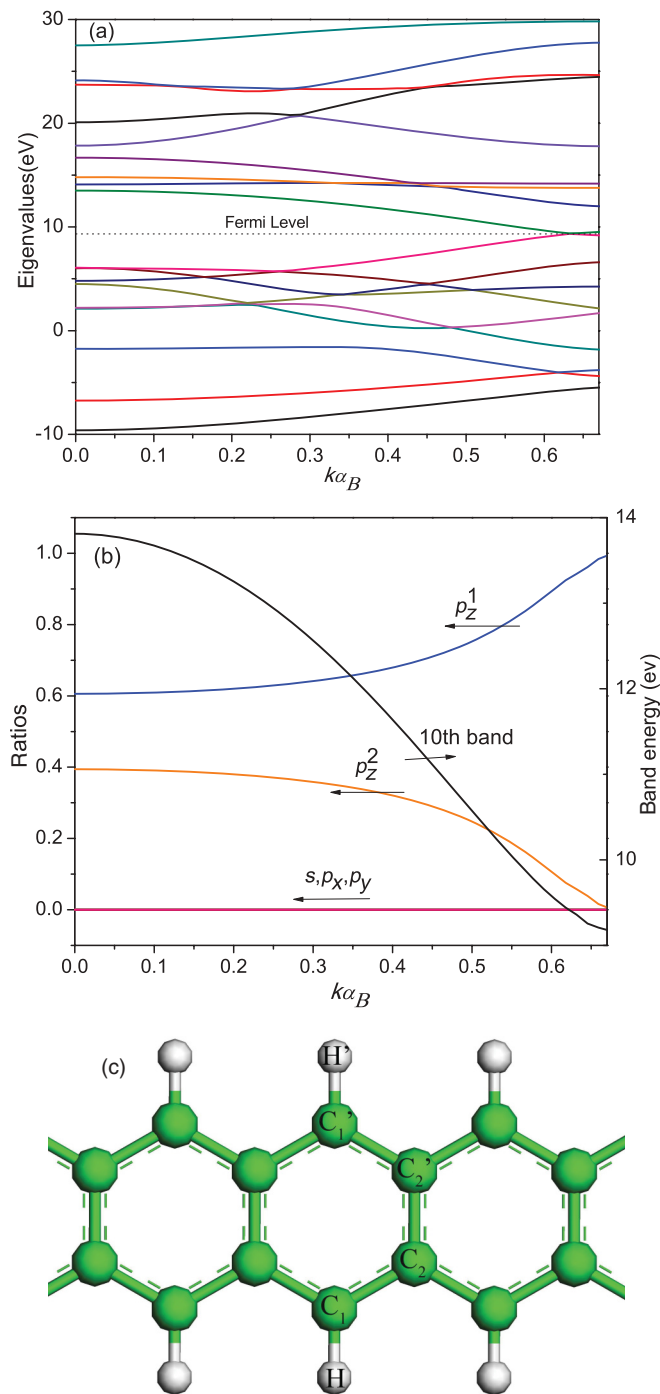


FIG. 14. (Color online) (a) Band structure (energy vs wave vector k) for each of the 18 eigenmodes of an infinite periodic system of period $a = 2.4$ Å (part of which is shown in [c]). The primitive cell consists of the 4 carbon atoms labeled C1, C1', C2, and C2' and 2 hydrogen atoms labeled H and H'. Each carbon atom contributes 4 atomic orbitals (3 p 's and 1 s), while each hydrogen atom contributes 1 s orbital. The top of the VB is partly the ninth band (counted at $k = 0$) up to $k = 0.26$ and partly the seventh band for $k > 0.26$. The bottom of the conduction band is the tenth band, consisting mainly of the p_z orbital located at carbon atom 1 as shown in (b), where the probability of finding the electron in each of the 18 atomic orbitals (left axis) is plotted, as well as the energy vs k (right axis). In (a), notice the Dirac point where the 7th and the 10th bands cross each other.

corners may possibly be obtained by a variation of the linear polymerization along the natural direction by making an angle of 60° . Possibly the interruption of the electronic flow will be more efficient if the nitrogen (or iron, as in Fig. 16) substitution takes place at the benzene(s) located at the corner (or corners of the molecule). One can envision one or two pairs of neighboring foreign atoms substituting for two or four carbon atoms of the corner benzene monomer. The question of the appropriate substrate and its role requires a serious quantum mechanical calculation or, better, a systematic experimental investigation of various substrates after the molecule has been synthesized. However, one can envision a high concentration of the ring-type molecules (shown in Fig. 9) within a proper solvent possibly oriented parallel to each other with the help of magnetic atom substitution (e.g., iron, as in Fig. 16). Finally, the assumption of a lossless classical ohm-type response has to be examined in the framework of quantum mechanics. We attempt such an examination in the next section.

IV. QUANTUM CONSIDERATIONS

First, we point out that in a recent experimental paper,³⁵ it was shown that Ohm's law survives to the atomic scale in a system of dopants four-atoms-wide, one-atom tall, and 106-nm-long in silicon. This system is essentially of the same width and height and of similar length as ours shown in Fig. 9. Thus, we expect a similar overall behavior, although the atomic details of the current distribution among the carbon atoms may differ from the classical one as a result of interference. Our explicit results, presented here, confirm this expectation.

We studied four systems: A relatively small-size ring molecule shown in Fig. 9(a), a straight segment of such a molecule consisting of carbon atoms and hydrogen atoms, a segment of the same size but with one 60° corner in the middle, and an infinite-size straight-line system. Although the first system is directly relevant to the quantum mechanical response of our ring molecules to the ac-EM field, we did also study the second and the third systems. This was done in order to clarify the role of the reflection at the edges of the second system and the role of the reflection and the transmission at the corner of the third system. This verifies that the ac-EM field excites a finite number of Bloch waves moving in both directions interfering among themselves and giving rise to the wave function pattern observed in the first system. We also studied the infinitely long straight-line system to reveal possible effects associated with very large ring molecules not accessible to the accurate direct technique applied to the first system. The infinite system reveals also interesting aspects of the Bloch waves propagating in it without the complicating interference effects due to more than one Bloch wave.

For the latter, we calculated the band structure, i.e., the energy vs crystal momentum for each of the 18 bands as well as the corresponding wave functions using the NRLTB method. The results for E vs k are shown in Fig. 14(a) and are reminiscent of the graphene dispersion relation. For the undoped case, the Fermi level coincides with the Dirac point

located near the boundary of the Brillouin zone (BZ). The dispersion relation near the Dirac point is linear for both the hole branch as well as electron branch with a velocity of about 700 km/s, i.e., almost three orders of magnitude lower than that of light. The optical gap at the center of the BZ is quite substantial around 8.5 eV. For k larger than 0.26 (in atomic units of k , where the edge of the BZ, π/a , is 0.69, and a is the period), the hole branch (HOMO) is mainly of p_z nature, mostly located at the carbon labeled 1 (see Fig. 14). The probability of being found at the carbon labeled 2 varies from 0.33 for k between 0.26 and 0.4 and gradually drops to zero as one approaches the boundaries of the BZ. The LUMO (electron) branch behaves in a similar way over the whole extent of the BZ [see Fig. 14(b)]. We conclude first that quantum mechanics preserves the ballistic and hence the lossless character of the transport within the assumption of negligible electron-phonon effects (and in the absence of interband transitions to be discussed later herein). This is a direct consequence of the exact periodicity of the system (in the absence of electron-phonon interactions and as long as interband transitions do not set in). The Dirac character of the electrons and holes near the Fermi level is expected to reduce the electron-phonon scattering, as a result of Klein's paradox (see, e.g., S. Flugge, *Practical Quantum Mechanics*, Springer, 1994). This expectation is verified in nanoribbons, where transport has been shown to be ballistic. Furthermore, Ref. 36 predicts ballistic transport in nanoribbons in spite of taking into account electron-phonon scattering as the most significant contribution to the mean free path. Moreover, there are theoretical investigations^{37,38} demonstrating that electron-phonon scattering in graphene is practically negligible; there are also graphene applications^{36,39} accepting a very weak electron-phonon scattering. In contrast, experimental studies^{40,41} (and references therein) seem to imply a more substantial loss below the frequency for interband transitions. However, this loss may be due to static impurities, point defects, edge scattering due to dangling carbon bonds, and their effect on electron-phonon scattering.

In view of the established almost negligible effect of the electron-phonon interaction per se^{37,38} and the fact that our system is stable and free of point defects, impurities, and dangling bonds, we conclude that quantum mechanics implies that the transport in our systems is of ballistic character, since no mechanism is left to destroy this character.

Thus, quantum mechanics will retain the ballistic character of the transport. The only modifications that quantum mechanics will bring to our classical ballistic transport for molecules (where their linear size is of the order of a few tens of nanometers) in the unbiased case are in the details as discussed next: One such detail is that the ballistic transport near the Fermi level will be mostly along the p_z orbital of carbons labeled 1 and not from p_z1 to p_z2 to p_z1 and so on. This partial elimination of a transport channel is expected to possibly reduce the imaginary part of the ac conductivity or, equivalently, the real part of the permittivity. Another modification, a very beneficial one for our purposes, is the strong suppression of the interband transitions by a factor equal to the square of the product of the p_z2 amplitude times the overlap of the p_z orbitals at neighboring carbon atoms 1 and

2. The reason for this is that the interband transition involves a matrix element of the form

$$\begin{aligned} & |(a_1\phi_{1z} + a_2\phi_{2z}|x|a_1\phi_{1z} + a_2\phi_{2z})|^2 \\ & = |a_1^*a_2\langle\phi_{1z}|x|\phi_{2z}\rangle + a_2^*a_1\langle\phi_{2z}|x|\phi_{1z}\rangle|^2, \end{aligned} \quad (4.1)$$

where it was taken into account that the diagonal matrix elements $\langle\phi_{iz}|x|\phi_{iz}\rangle$ $i = 1, 2$ are equal to zero for reasons of symmetry. Keep in mind that a_2 tends to zero as the Fermi energy is approached, i.e., for low frequencies, which implies that the low-frequency absorption gap is much larger than the density of states (DOS) gap for very large unbiased ring molecules of the type shown in Fig. 9. In any case, the interband transitions up to a frequency $\omega = 2$ eV/ \hbar can become zero as a result of Pauli's principle by biasing the system by a voltage V , which can be as high as 1.4 V. This is a common practice in graphene.³⁶ We point out that the changes in the current distributions produced by quantum mechanical effects are of minor quantitative effects in the high-frequency EM response. Actually, the quantities that are relevant for use in our systems as high-frequency metamaterials are their overall resistance R , their overall self inductance $L = L_m + L_e$, and the capacitance C (appearing only when the continuity of the flow is interrupted by proper doping, as will be discussed later on). Next, we show that R is zero for frequencies below the interband transitions (assuming negligible electron-phonon scattering); this almost lossless operation is a very important point and the basic reason for considering the bottom-up molecular approach for optical metamaterials. The kinetic contribution L_e to the self inductance is given by $L_e = \text{cons} \cdot l$, where l is the overall length of the ring molecule, and the constant is equal to m_e/e^2n_eS ; n_e is the concentration of carriers, and S is the constant effective cross section of the ring molecule of the order of $3 \times 4 \text{ \AA}^2$. Thus, L_e is independent of the details of the distribution of the current density. The magnetic contribution L_m to the self inductance as discussed in the introduction will be of the form $L_m = (a_1\mu_0/2\pi) \cdot l \cdot \ln(a_2l/\sqrt{S})$, where a_1 and a_2 are dimensionless parameters of the order of one depending on the current-density distribution in the ring molecule. However, since L_e is four orders of magnitude larger than L_m , the exact values of a_1 and a_2 are completely irrelevant for our purposes.

To directly substantiate our claim that $R \approx 0$, we performed very accurate quantum mechanical calculations on the molecule shown in Fig. 9(a) and the other two auxiliary systems mentioned at the beginning of the present Sect IV. These calculations were done by a first-principles, DFT-based NRLMOL method, which, as a trade-off for its reliability, does not allow substantially larger molecules than that of Fig. 9(a). We obtained the energy levels (and hence the DOS), the corresponding energy eigenfunctions, their s or p character, and the absorption coefficient, which by the Kramers-Kronig relation allows us to determine the permittivity. These systems, because of their small size, exhibit a gap larger than 2.0 eV, reaching an estimated 3.25 eV depending on the system. The energy eigenfunctions are periodic, consisting of opposite-traveling Bloch waves mostly along the external and the

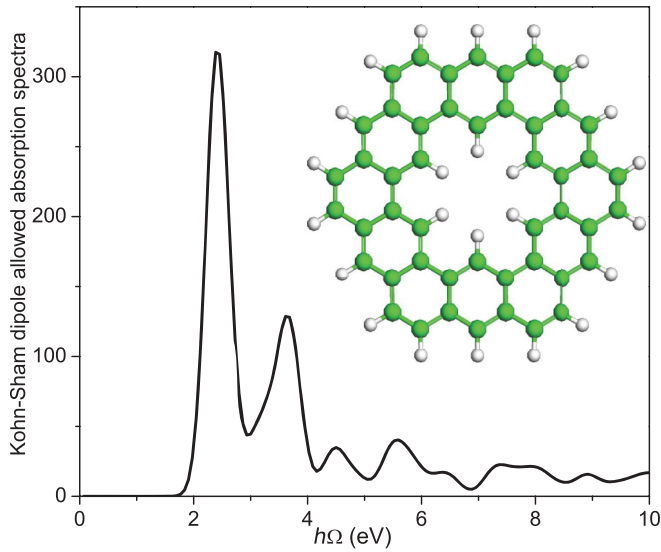


FIG. 15. (Color online) Plot of absorption coefficient (in arbitrary units) vs $\hbar\omega$ for the ring molecule $C_{48}H_{24}$ shown above, calculated by the DFT method NRLMOL. The shown gap of 2 eV is expected to be larger, for two reasons: (1) because the small imaginary part introduced to smoothen the plot lowers the gap from 2.5 eV to 2 eV; and (2) because it is known that DFT approaches produce gaps about 30% lower than the actual ones.

internal edges of the molecule—a result further supporting our conclusion of ballistic transport.

However, the definite proof (within the generally accepted almost negligible electron-phonon scattering) of the ballistic character of transport in our ring molecule, i.e., that $R \approx 0$, is shown in Fig. 15, where we plot the absorption coefficient vs frequency $\hbar\omega$. This first-principles, very accurate quantum-mechanical calculation shows that there is a gap where the absorption coefficient is exactly zero. This is a direct proof that the losses are exactly zero up to the set-in of the interband transitions (which appear at almost 2 eV for this size of molecule), and, consequently, the transport is ballistic. We point out again that the reason a molecular approach to metamaterials was proposed is exactly the expected (and established in this paper) superiority in comparison with the metallic top-down scheme as far as losses are concerned. As the size of the ring molecule increases (see Fig. 9), the gap in the density of states (DOS) becomes narrower and eventually, for infinite systems, closes, as shown in Figs. 9(b) and 14. The latter shows that the closing of the gap is similar to that in graphene with the Dirac point and the linear E vs k behavior around it. Notice, however, that the gap in the absorption coefficient is expected to be larger than that of DOS and may not close for nanometer-size molecules, because of the presence of the small matrix element incorporated in the absorption coefficient, as we mentioned before. Finally, we point out that the knowledge of the absorption coefficient allows the calculation of the permittivity through the Kramers-Kronig relations. We emphasize once more that the existing differences between the classical and the quantum calculations in high-frequency current-density distributions (some of which we pointed out before) will have practically no effect on

the resistance R and the self inductance L of our ring molecule.

V. DISCUSSION AND CHECKS

In this section, we briefly review some of the other assumptions underlying the possibility of a graphene-based approach to the construction of a molecular SRR or other types of optical “atoms.”

The first concern is whether a doped graphene-based molecule retains its planar structure or if its coordination within the plane is retained as the size of the molecule and the concentration of dopants are increased.

We found that the answer to both of these questions is an encouraging “yes” for relatively low or even medium concentrations of nitrogen dopants. For other dopants, such as boron, aluminum, iron, and oxygen, there is considerable coordination rearrangement, although the planar structure seems to be perfectly retained, as shown in Fig. 16. It is worthwhile to point out that doping by iron offers the possibility of magnetically orienting the molecules within a proper solvent, conceivably creating a close-packed lattice, which can substantially lower the permeability as we mentioned before (see Fig. 6).

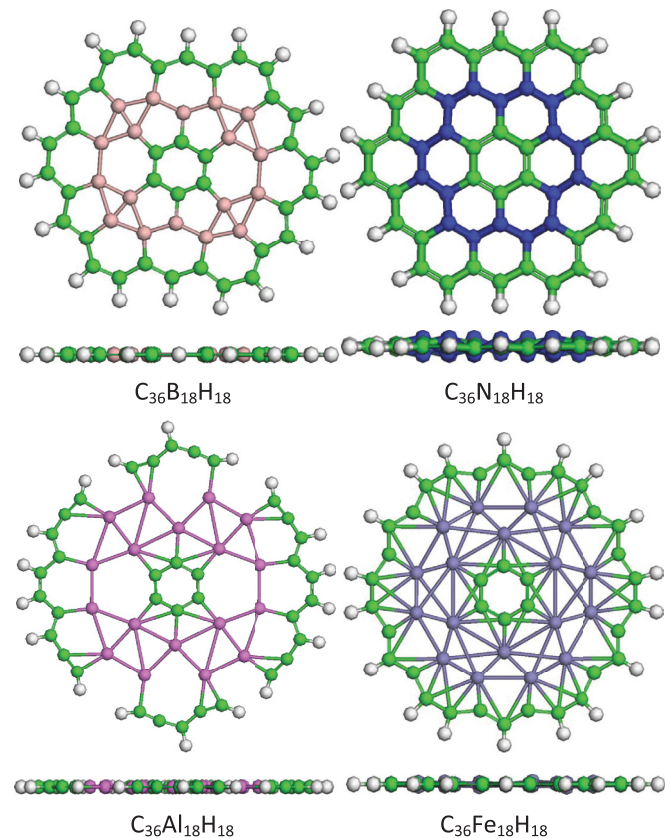


FIG. 16. (Color online) Two views of each of the three molecules $C_{36}B_{18}H_{18}$, $C_{36}Al_{18}H_{18}$, and $C_{36}Fe_{18}H_{18}$. The $C_{36}N_{18}H_{18}$ molecule is also shown for comparison. The B, Al, Fe, and N atoms and their bonds are shown in different colors online. Notice the perfect planar structure of the first three molecules in spite of the extensive bond rearrangement.

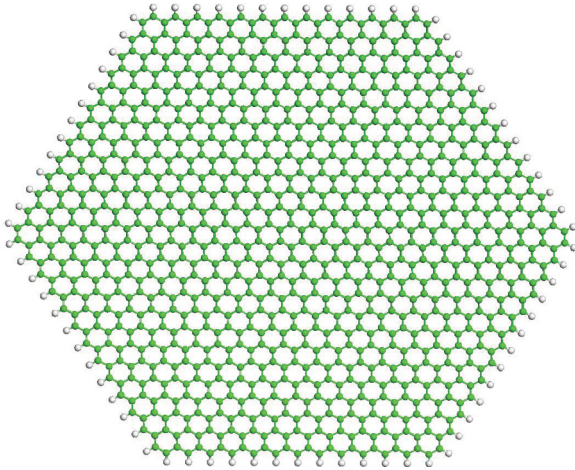


FIG. 17. (Color online) A $C_{1014}H_{78}$ graphene-based molecule, which, in combination with an identical one, can form a “slab-pair” element exhibiting a resonance response equivalent to a resonant circuit.

The second question—a very important one—is the following: Is a dopant or a cluster of dopants capable of blocking the flow of p_z electrons through it? The simulation by a perfect metallic wire mesh with some sites missing, as shown in Figs. 7, 8, and 10, is based on the assumption that the answer to this crucial question is yes. Our calculations, although they do not provide a direct definite answer, indicate that the blocking is probably only partial. Indeed, although the dopant does create a bound localized state around it, its characteristic decaying length is larger than the nearest neighbor distance, showing that a larger cluster of dopants may possibly provide the desired blocking of the electronic flow. Such a cluster is easily incorporated, at least in principle, in molecules shown in Fig. 9. This picture of only partial blocking by a single dopant is further supported by calculations of the polarizability and the aromaticity index of the molecules. These calculations show that there is no considerable reduction of either the polarizability or the aromaticity index by doping, at least with nitrogen. Recent experimental results⁴² confirm this picture of partial blocking by nitrogen atoms. Thus, it seems that either a large cluster of nitrogen atoms or, possibly, other dopants may offer the capacitive-element in a graphene-based molecular SRR. We intend to pursue this cluster approach of nitrogen or trivalent dopants by developing numerical codes within our NRLMOL or TB schemes, which will calculate the circular current flow in the presence of an ac magnetic field perpendicular to the plane of the graphene-based molecules.

It must be pointed out that, in addition to SRR-type molecular elements for bottom-up metamaterials, which seem so promising, undoped large graphene-based molecules, such as shown in Fig. 17, can be used in the “slab-pair” configuration,^{43,44} which has been shown to be quite successful in obtaining high operational frequency with relatively high figure of merit. The latter is by definition the ratio $\text{Re}\chi_m/\text{Im}\chi_m$ and, as was mentioned in the introduction, must exceed ~ 10 for practical applications.

Moreover, we have shown that undoped single-wall nanotubes may offer a resonant response to EM waves in the soft

x-ray range. This is an exciting possibility for constructing metamaterials in the extreme ultraviolet (UV) or the soft x-ray part of the spectrum.

VI. SUMMARY

In this paper, we presented a first investigation of a molecular bottom-up approach to the optical negative index or other types of high-frequency metamaterials. We studied graphene-based molecules, demonstrating that the flow of the p_z electrons is ballistic and not diffusive, as in metals, even the most conductive of them. The expected drastic reduction in ohmic losses opens up the possibility of a high figure of merit for optical, UV, and even soft x-ray metamaterials.

We employed the DFT-based code NRLMOL to obtain the eigenstates and eigenenergies of a large number of graphene-based molecules, including nanotubes, of various shapes and sizes, both undoped and doped with nitrogen or trivalent atoms. The NRLTB, where the parameters were fit to first-principles results, allows us to study the spectrum, the eigenfunctions, and the stability of molecules with several thousand atoms.

We presented accurate, first-principles, quantum mechanical calculations confirming the picture of ballistic electronic flow in our ring molecules shown in Fig. 9 (within the generally accepted notion of almost negligible electron-phonon scattering). We assumed that the dopants will block the flow of p_z electrons—a doubtful assumption that may become realistic if the pair of dopants is replaced by an appropriate cluster of them. Recent experiments³⁵ support our quantum mechanical calculations showing that the overall flow of electrons under the action of an EM field obeys Ohm’s law with almost zero resistance, although the quantum distribution of the current may be different than the one obtained by our classical approach. Anyway, this difference has no measurable effect on either the self inductance or the resistance; these quantities determine the performance of the ring molecule as element of optical metamaterials.

Accepting ballistic flow and assuming that dopants will block the flow of p_z electrons—an assumption to be tested—we have simulated the response of the molecule to an EM wave by a network of perfect metallic wires with or without some sites missing. This let us calculate the induced currents and the induced EM fields. We expect that the overall flow obtained through this simulation will fairly represent the flow in the real molecule, although the details regarding the local distribution of currents and fields may be different. We also expect that even if a single dopant fails in blocking the flow of p_z electrons, a cluster of dopants can do the job. Thus, molecules of the type shown in Fig. 9 are good candidates for molecular SRRs. Notice also that the molecule shown in Fig. 9(a), known as kekulene, has been synthesized.³⁵ In addition, large undoped molecules as in Fig. 17 are very promising for molecular LHMs based on the slab-pair configuration.

We found an exciting possibility of resonant response of single-wall undoped carbon nanotubes at soft x rays or, possibly, at extreme UV, where the resonance frequency may depend on the interplay of the lengths, a , λ , and d , where d is the linear size of the benzene ring.

ACKNOWLEDGMENTS

The authors would like to acknowledge support by the US Air Force via Grant S-876-060-007 with UES Inc. and by

Office of Naval Research (ONR) Grant N00014-09-1-1025, and the European Union (EU) through the grants ENSEMBLE, NIMNIL, BY-NANOERA, and the COST Action MP0803.

- ¹V. G. Veselago, *Sov. Phys. Usp.* **10**, 509 (1968).
- ²C. M. Soukoulis, M. Kafesaki, and E. N. Economou, *Adv. Mater.* **18**, 1941 (2006).
- ³D. R. Smith, J. B. Pendry, and M. C. K. Wiltshire, *Science* **305**, 788 (2004).
- ⁴J. B. Pendry, *Opt. Express* **11**, 639 (2003).
- ⁵J. B. Pendry, A. J. Holden, D. J. Robbins, and W. J. Stewart, *IEEE Trans. Microwave Theory Tech.* **47**, 2075 (1999).
- ⁶C. M. Soukoulis, S. Linden, and M. Wegener, *Science* **315**, 47 (2007).
- ⁷V. M. Shalaev, *Nat. Photonics* **1**, 41 (2007).
- ⁸C. M. Soukoulis and M. Wegener, *Science* **330**, 1633 (2010).
- ⁹J. B. Pendry, *Phys. Rev. Lett.* **85**, 3966 (2000).
- ¹⁰D. R. Smith, W. J. Padilla, D. C. Vier, S. C. Nemat-Nasser, and S. Schultz, *Phys. Rev. Lett.* **84**, 4184 (2000).
- ¹¹R. A. Shelby, D. R. Smith, and S. Schultz, *Science* **292**, 77 (2001).
- ¹²C. G. Parazzoli, R. B. Gregor, K. Li, B. E. C. Koltenbah, and M. Tanielian, *Phys. Rev. Lett.* **90**, 107401 (2003).
- ¹³K. Li, S. J. McLean, R. B. Gregor, C. G. Parazzoli, and M. H. Tanielian, *Appl. Phys. Lett.* **82**, 2535 (2003).
- ¹⁴M. Bayindir, K. Aydin, E. Ozbay, P. Markos, and C. M. Soukoulis, *Appl. Phys. Lett.* **81**, 120 (2002).
- ¹⁵K. Aydin, K. Guven, M. Kafesaki, L. Zhang, C. M. Soukoulis, and E. Ozbay, *Opt. Lett.* **29**, 2623 (2004).
- ¹⁶J. Zhou, T. Koschny, M. Kafesaki, E. N. Economou, J. B. Pendry, and C. M. Soukoulis, *Phys. Rev. Lett.* **95**, 223902 (2005).
- ¹⁷E. N. Economou, M. Kafesaki, C. M. Soukoulis, and T. Koschny, *J. Comput. Theor. Nanosci.* **6**, 1827 (2009).
- ¹⁸C. M. Soukoulis, T. Koschny, J. F. Zhou, M. Kafesaki, and E. N. Economou, *Phys. Status Solidi B* **244**, 1181 (2007).
- ¹⁹L. Solymar, *Lectures on Electromagnetic Theory: A Short Course for Engineers* (Oxford University Press, London, 1976).
- ²⁰L. D. Landau, E. M. Lifshitz, and L. P. Pitaevskii, *Electrodynamics of Continuous Media* (Pergamon, Oxford; New York, 1984).
- ²¹D. O. Guney, T. Koschny, and C. M. Soukoulis, *Phys. Rev. B* **80**, 125129 (2009).
- ²²R. S. Penciu, M. Kafesaki, T. Koschny, E. N. Economou, and C. M. Soukoulis, *Phys. Rev. B* **81**, 235111 (2010).
- ²³P. Tassin, L. Zhang, T. Koschny, E. N. Economou, and C. M. Soukoulis, *Phys. Rev. Lett.* **102**, 053901 (2009).
- ²⁴A. Fang, T. Koschny, and C. M. Soukoulis, *Phys. Rev. B* **82**, 121102 (2010).
- ²⁵A. Fang, T. Koschny, M. Wegener, and C. M. Soukoulis, *Phys. Rev. B* **79**, 241104 (2009).
- ²⁶S. Wuestner, A. Pusch, K. L. Tsakmakidis, J. M. Hamm, and O. Hess, *Phys. Rev. Lett.* **105**, 127401 (2010).
- ²⁷S. M. Xiao, V. P. Drachev, A. V. Kildishev, X. J. Ni, U. K. Chettiar, H. K. Yuan, and V. M. Shalaev, *Nature* **466**, 735 (2010).
- ²⁸N. Meinzer, M. Ruther, S. Linden, C. M. Soukoulis, G. Khitrova, J. Hendrickson, J. D. Orlitzky, H. M. Gibbs, and M. Wegener, *Opt. Express* **18**, 24140 (2010).
- ²⁹M. R. Pederson, D. V. Porezag, J. Kortus, and D. C. Patton, *Phys. Status Solidi B* **217**, 197 (2000).
- ³⁰R. E. Cohen, M. J. Mehl, and D. A. Papaconstantopoulos, *Phys. Rev. B* **50**, 14694 (1994).
- ³¹M. J. Mehl and D. A. Papaconstantopoulos, *Phys. Rev. B* **54**, 4519 (1996).
- ³²N. Bernstein, M. J. Mehl, D. A. Papaconstantopoulos, N. I. Papanicolaou, M. Z. Bazant, and E. Kaxiras, *Phys. Rev. B* **62**, 4477 (2000).
- ³³D. A. Papaconstantopoulos, M. J. Mehl, S. C. Erwin, and M. R. Pederson, in *Material Research Society Proceedings Tight-Binding Approach to Computational Materials Science*, edited by P. Turchi, A. Gonis and L. Colombo (Materials Research Society, Boston, 1998), p. 221.
- ³⁴D. Finkenstadt, G. Pennington, and M. J. Mehl, *Phys. Rev. B* **76**, 121405(R) (2007).
- ³⁵B. Weber, S. Mahapatra, H. Ryu, S. Lee, A. Fuhrer, T. C. G. Reusch, D. L. Thompson, W. C. T. Lee, G. Klimeck, L. C. L. Hollenberg, and M. Y. Simmons, *Science* **335**, 64 (2012).
- ³⁶F. H. L. Koppens, D. E. Chang, and F. J. G. de Abajo, *Nano Lett.* **11**, 3370 (2011).
- ³⁷D. Gunlycke, H. M. Lawler, and C. T. White, *Phys. Rev. B* **75**, 085418 (2007).
- ³⁸K. M. Borysenko, J. T. Mullen, E. A. Barry, S. Paul, Y. G. Semenov, J. M. Zavada, M. B. Nardelli, and K. W. Kim, *Phys. Rev. B* **81**, 121412 (2010).
- ³⁹A. Vakil and N. Engheta, *Science* **332**, 1291 (2011).
- ⁴⁰D. K. Efetov and P. Kim, *Phys. Rev. Lett.* **105**, 256805 (2010).
- ⁴¹P. Tassin, T. Koschny, M. Kafesaki, and C. M. Soukoulis, *Nat. Photonics* **6**, 259 (2012).
- ⁴²L. Y. Zhao, R. He, K. T. Rim, T. Schiros, K. S. Kim, H. Zhou, C. Gutiérrez, S. P. Chockalingam, C. J. Arguello, L. Pálová, D. Nordlund, M. S. Hybertsen, D. R. Reichman, T. F. Heinz, P. Kim, A. Pinczuk, G. W. Flynn, and A. N. Pasupathy, *Science* **333**, 999 (2011).
- ⁴³V. M. Shalaev, W. S. Cai, U. K. Chettiar, H. K. Yuan, A. K. Sarychev, V. P. Drachev, and A. V. Kildishev, *Opt. Lett.* **30**, 3356 (2005).
- ⁴⁴J. F. Zhou, E. N. Economou, T. Koschny, and C. M. Soukoulis, *Opt. Lett.* **31**, 3620 (2006).
- ⁴⁵H. A. Staab and F. Diederich, *Chem. Ber.* **116**, 3487 (1983).